ELSEVIER

Materials Science and Engineering B96 (2002) 94–101

MATERIALS SCIENCE & ENGINEERING B

www.elsevier.com/locate/mseb

Strain engineering, self-assembly, and nanoarchitectures in thin SiGe films on Si

A.R. Woll *, P. Rugheimer, M.G. Lagally

University of Wisconsin, Madison, WI, USA

Abstract

We review recent experimental results pertaining to the self-assembly and self-ordering of quantum dots (QDs) in semiconductor systems. In particular, we focus on attempts to control the density, size, and size distributions of strained islands, both within a single strained layer and in quantum dot multilayers. We also discuss the factors affecting vertical ordering in multilayers such as the nature of the strain field produced by buried islands and the thickness of the spacer layer. © 2002 Elsevier Science B.V. All rights reserved.

Keywords: Self-assembly; Self-ordering; Quantum dot (QD)

1. Introduction

Most proposed electronic or opto-electronic devices involving quantum dots (QDs) require that a large number of QDs be made with identical or nearly identical properties. In this paper we describe ways to manipulate and optimize an ensemble of three-dimensional (3D) islands. First we discuss self-organization and methods of control within a single layer of 3D islands. We then focus on the growth of quantum dot multilayers: multiple layers of 3D islands, separated by spacer layers, consisting of the substrate material, which completely cover the islands so that the surface becomes almost as smooth as the original substrate. The lateral compositional inhomogeneity caused by the buried islands is transmitted to the surface through strain, so that nucleation of the second and subsequent quantum dot layers is no longer spatially random. QDs prepared this way exhibit increasing degrees of order, size, shape, and position as more layers are added.

* Corresponding author
E-mail address: lagally@engr.wisc.edu (A.R. Woll).

2. Single layers

The characteristics of 3D, coherent islands that most influence their electronic and optical properties are size, size uniformity, and number density. Independent control of these parameters would allow quantum dot layers to be tailored for specific devices, but represents a significant challenge. In the following sections we describe work aimed at achieving such control.

2.1. Size and size distributions

The size distribution of coherent 3D islands can be quite narrow, but is very sensitive to growth parameters. For example, using AFM, Drucker et al. [1] compared the base lengths of pyramidal Ge islands on Si(001). The mean base length was ≈ 70 nm, while the full width at half maximum (FWHM) of the distribution of base lengths about the mean was 25%. Varying the growth temperature from 550 to 450 °C caused the island base-length distribution to broaden to $\approx 40\%$. The narrow size distribution in Ge/Si has been attributed to kinetically self-limited growth.

0921-5107/02/$ - see front matter © 2002 Elsevier Science B.V. All rights reserved.
PII: S0921-5107(02)00298-2

Because the shape transformation of Ge/Si 3D islands, it can be difficult to avoid a bimodal size distribution, in which both small ‘pyramids’ as well as larger ‘domes’ are present. Ross et al., using in situ TEM, empirically determined a procedure to produce a monomodal size distribution of coherent domes [2] having a FWHM of only 15%. When domes first appear, their size distribution is relatively narrow. If deposition is stopped at this stage, and the Ge/Si film is annealed, all pyramidal islands will eventually disappear as their atoms diffuse to domes, whose chemical potential is lower [2]. Once all pyramids disappear the size distribution is no longer bimodal, and the size distribution of domes is minimized. Further annealing results in coarsening the growth of larger domes at the expense of slightly smaller ones, broadening the size distribution and, eventually, leading to dislocation formation. Thus the narrowest size distribution is obtained if the temperature is reduced just after all pyramids disappear.

For InAs/GaAs [3,4] and PbSe/PbTe [5], typical size distribution widths are in the range of 7–15% of the mean island size for islands with mean base sizes of ≈ 30 nm. The evolution of 3D coherent islands in these systems differs qualitatively from that of SiGe/Si in at least three important ways: First, the island size distribution in these systems is monomodal rather than bimodal. Also, the mean island size does not increase monotonically during growth [3–5]. Finally, the island size distribution in InAs/GaAs can become narrower during annealing [6]. These observations suggest that narrow island size distributions are more easily achieved in InAs/GaAs and PbSe/PbTe than in SiGe/Si.

As in the Ge/Si system, island size distributions in III–V systems are very sensitive to growth conditions. In [4], it is shown that differences of as little as 0.08 ML coverage result in a broadening of the size distribution from ≈ 10 to 60% of the mean base size of InAs islands on GaAs. This sensitivity arises, evidently, from island-to-island interactions [4]. The island size distribution is broad in the early stages of growth, when islands are relatively sparse. As the island density increases, the mean island size and size distribution width both decrease. The precise relationship between island density and island size distribution is not yet understood.

2.2. Island density

The number density of coherent, 3D islands in SK systems varies qualitatively with temperature T and deposition flux F in the same way as nucleation in ordinary, Volmer-Weber (VW) systems [7]: the density goes as $(F/D)^x$, where D is the diffusion constant, which depends exponentially on T, and x is positive and depends on the details of the system. Such a dependence has been observed both for SiGe/Si(001) [8] and for InAs/GaAs [9]. Thus density increases with increasing flux and decreases with increasing temperature. In SiGe/Si(001), the number density of coherent, 3D islands has been manipulated from about 10^8–10^{12} islands cm^{-2} [8,10–12]. The 3D island density also depends sensitively on the total coverage within a certain coverage range. For InAs/GaAs, the appearance of 3D coherent islands is very sudden. At a growth rate of ≈ 0.01 ml s^{-1}, the 3D island density changes from zero at 1.5 ml to $\approx 10^{10}$ cm^{-2} at 1.7 ml [3,4].

2.3. Lateral position

Many potential applications for QDs require precise control not only over their shape, size, and size distribution, but also over their lateral position. Recently, an increasing effort has been devoted to finding new methods to achieve such control over self-assembled, 3D coherent islands. Most of these entail the use of the substrate as a template for island nucleation, through lithography defined surface morphology [13–19], surface steps or step bunches [18,20–23], or the intentional formation of dislocations [24].

Kamins et al. [15,17] deposited Ge islands on raised Si strips on a (001) wafer. Valleys were etched through a SiO_2 layer down to the silicon and parallel to the ⟨100⟩ direction. Using CVD, Si was then selectively deposited on regions of exposed Si, resulting in raised Si strips bounded by {011} side walls. For strips varying in width from 450 nm to 1.7 μm, islands nucleated preferentially at the edges, forming a linear array, and had square bases with a mean side length of 86 nm and a mean height of 15 nm.

Jin et al. also investigated the arrangement of Ge islands on lithographically patterned sub-micron mesas [13,14]. Fig. 1 shows a variety of patterned mesas on Si(001) and the arrangement of 3D Ge islands grown on top of them. Long, raised stripes result in extremely uniform islands growing in long, ordered arrays, similar to the results of Kamins et al. Deposition of 9 ml of Ge on raised, square mesas results in the formation of islands at each corner. Further deposition results in the formation of a fifth, smaller island in the center. These results demonstrate the feasibility of using lithography to control the positions at which Ge islands nucleate on a Si substrate.

Recently, Rugheimer et al. [19] investigated Ge deposition on raised Si mesas with dimensions of 3–20 μm on both bulk Si(001) and silicon-on-insulator (SOI) substrates. These mesas were fabricated by a single patterning step followed by a reactive ion etch, and are thus bounded by nearly vertical side walls, rather than low-index facets. At a deposition temperature of 700 °C, the distribution of coherent, pyramidal islands during early stages of deposition appears to be unaffected by the mesa edge. Beyond a certain size,

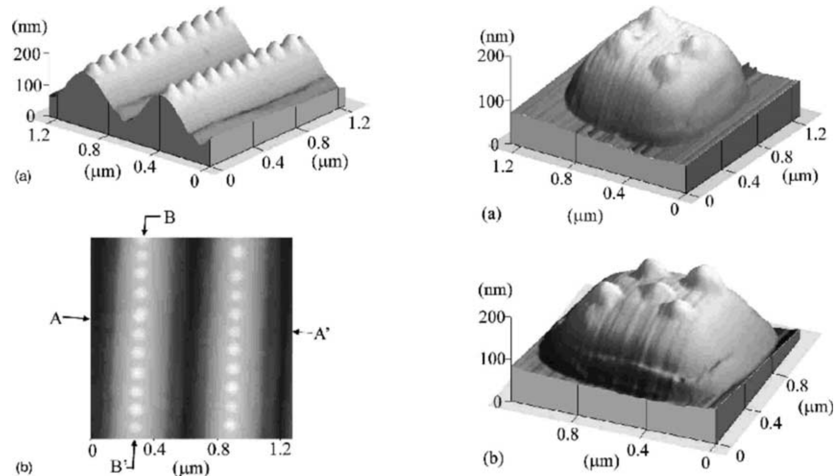

Fig. 1. (Left) AFM images of self-organised 3D Ge dome-shaped on ⟨110⟩-oriented Si stripe mesas with a period of 0.6 μm. (Right) Ge domes on square Si mesas with base lines parallel to ⟨110⟩ directions. The Ge thickness is (a) 9 ml and (b) 10 ml. The average island base size is 140 nm. Reprinted from [13] with the kind permission of the authors.

however, islands at edges dominate the coarsening process. At this temperature, intermixing also occurs: large islands at the edge deplete not only Ge from nearby, smaller islands, but also Si from the surrounding substrate. For mesas fabricated on SOI with a ≈ 10 nm thick Si template layer, each large edge island absorbs all the Si from the substrate surrounding it, creating an isolated ring of SiGe islands at the mesa edge [19]. Once these islands have locally depleted the Si template layer, the process repeats itself as a new ring of isolated SiGe islands is formed inside the first one. Fig. 2 shows an AFM image of a mesa with three such 'island rings'. Cross-sectional TEM verifies that the 10 nm silicon layer between these 3D islands is completely removed down to the oxide, but remains intact underneath the

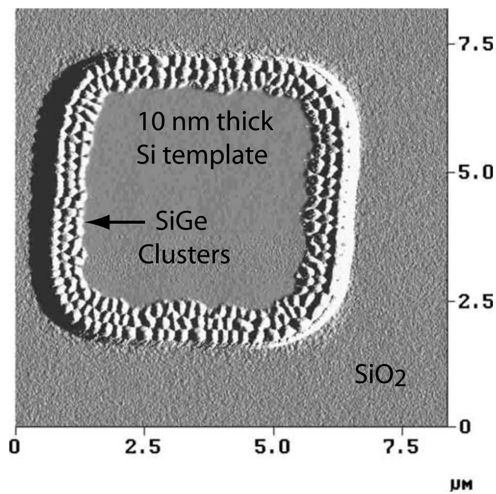

Fig. 2. AFM image of a raised 5 μm SOI mesa onto which 1.6 nm Ge has been deposited using MBE at a growth temperature of 700 °C. The Si template layer is 10 nm thick. The region around the mesa is oxide. The image is shown in differential mode.

3D islands. TEM results also indicate that these large islands contain no dislocations [19].

The use of patterning to manipulate the lateral position of 3D, coherent islands has also been applied to III–V systems [18,25]. Ploog et al. have demonstrated the controlled formation of quantum wires, QDs, and coupled wire-dot arrays of GaAs bounded by AlGaAs. Such control was achieved by combining lithographic techniques with methods to achieve step bunching on [311]A GaAs substrates.

Dislocations, like lithographically defined patterns, can act as preferred sites for island nucleation. Teichert et al. [24] exploited this phenomenon to create a highly ordered square array of pyramidal, {105}-faceted SiGe islands. Starting with a clean Si(100) surface, they grew 30 nm of $Si_{0.7}Ge_{0.3}$ at 150 °C in the presence of 1 keV Si^{+} ions, followed by conventional growth of 50 nm of additional alloy at 550 °C. The low temperature and ion bombardment during the first growth step result in the formation of a dense array of dislocations, which act as preferred sites for island nucleation. Fig. 3 shows AFM images of the resulting island array. The ordering is most pronounced in regions of highest dislocation density, such as the 1×1 μm region enlarged at the right. It is possible that the size of such well-ordered regions might be significantly increased by further augmenting the dislocation density.

3. Multilayers

Multilayers of coherent 3D islands not only offer opportunities to realize 3D arrays of QDs, but also provide an additional tool to explore the atomistic mechanisms of self-assembly through strain management. These multilayers are fabricated by alternating

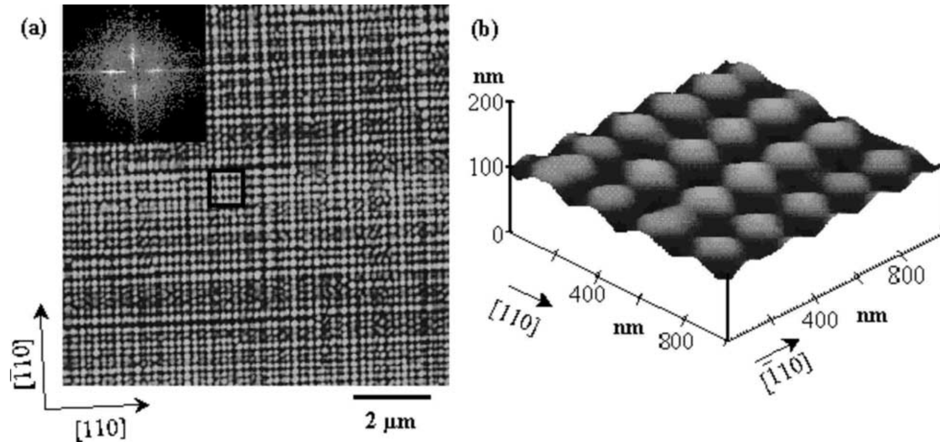

Fig. 3. Morphology of a 80-nm $Si_{0.7}Ge_{0.3}$ film, of which the first 30 nm was grown at 150 °C under simultaneous 1 keV Si^{+} ion bombardment. The remaining 50 nm was grown without ion bombardment at 550° C. (a) 10 × 10 µm image, gray-scale: 15 nm, inset: corresponding power spectrum ranging from −25.6 to 25.6 μm^{-1}. (b) 3D 1 × 1 µm image obtained with an electron-beam deposited tip of the area framed in (a). Reprinted from [24] with the kind permission of the authors.

heteroepitaxial layers with spacer layers of the substrate material. The spacer layer fills in the region between islands before covering them, so that the resulting surface is as smooth as the initial substrate. The lateral inhomogeneity due to buried islands is transmitted to the surface through strain, so that nucleation of 3D islands in the second and subsequent layers is no longer spatially random. By controlling the relative thicknesses of the two layers, the composition of the heteroepitaxial layer, the temperature at various stages of growth, and the deposition rate, 3D island sizes, shapes, size distributions, and spatial distributions can be modified and to some extent controlled. In all cases, 3D islands in multilayers are coherent with the substrate.

3.1. Basic concepts of multilayer ordering

The AFM images shown in Fig. 4 compare the arrangement of $Si_{0.25}Ge_{0.75}$ QD clusters in a single-layer film (a) and in the 20th SiGe layer of a Si–SiGe multilayer (b) grown on Si(001). All SiGe layers have a mean thickness of 2.5 nm, and are separated by spacer layers consisting of 10 nm Si. Analysis of both images reveals that the islands are bounded by {105} facets. The island size is larger in the multilayer film, with a concomitant decrease in island number density [26,27].

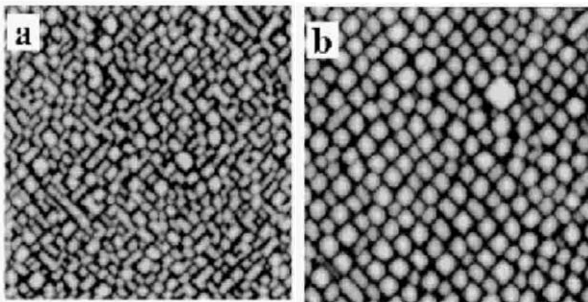

Fig. 4. AFM images of $Si_{0.25}Ge_{0.75}$/Si(001) superlattices. The horizontal direction corresponds to [110]. (a) 0.8 × 0.8 µm image of a single SiGe layer. Gray sacle range is 5 nm. (b) 1.25 × 1.25 µm image of the 20th SiGe layer. Gray scale range 10 nm. Reprinted from [26] with the kind permission of the authors.

The increased size of coherently strained 3D islands with increasing layer number is accompanied by an increased regularity, both in size distribution and position. The power spectrum of the images [27] shows a fourfold pattern in each case, arising from the short-range order of close-packed rectangular islands. However, the pattern from the multilayer surface is considerably sharper, and exhibits second-order peaks, indicating a much more regular array. Quantitatively, the width of the island size distribution, for these close-packed islands, may be estimated from the width of the first peak in the power spectrum along a {100} direction. It changes from ~ 1.1 to 0.3 $\langle L \rangle$ between Fig. 4a and b, where $\langle L \rangle$ is the average lateral size of the islands. It is also clear from the images that the island shape becomes more square for the multilayer film. The average aspect ratio (base length to width) of the islands changes from approximately 1.50 to 1.15 ± 0.05. Thus the increased regularity evident in Fig. 4 may be characterized by a narrowing in the distribution of island sizes and spacings, and by an evolution from rectangular to square island shapes [27].

Cross-sectional TEM measurements elucidate the ordering mechanism operative in Fig. 4. Fig. 5 shows a bright-field image [28] of a sample grown in a manner similar to that of Fig. 4b. Dark regions of the image correspond to SiGe alloy, while lighter regions correspond to the Si substrate and Si spacer layers. Islands appear to be stacked on top of one another, or vertically correlated. This phenomenon is a nearly ubiquitous feature of multilayer QD films [26–36].

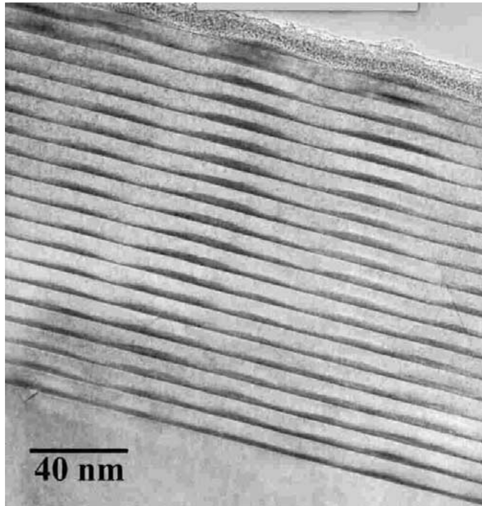

Fig. 5. Representative [110]-cross-section bright-field TEM micrograph of an uncapped 20 bilayer $Si_{0.25}Ge_{0.75}$/Si multilayer, showing the vertical ordering of the SiGe islands (from [28]).

In order for lateral ordering in island positions to occur, the vertical correlation evident in Fig. 5 cannot be absolute. If it were, subsequent layers in a multilayer film could only replicate the stochastic nucleation pattern of the first layer. The middle column of islands in Fig. 5 shows evidence for a gradual change in the arrangement of islands as the number of layers is increased. In particular, small islands move toward one another [28]. Once the pair of islands becomes close enough, only one island of larger size appears in the following layer. Subsequently, this island replicates itself without significant further changes in size or position [28].

Tersoff et al. proposed a simple model to explain the ordering observed in Fig. 4 [26]. Islands are treated as spherical inclusions in a continuum elastic medium of the substrate material buried at depth L below a film surface. The strain field at the surface is then calculated, and each minimum in the strain field with respect to the lattice parameter of the QD material is chosen for nucleation of islands in the current layer. In SiGe/Si multilayers, these regions will be under tensile strain

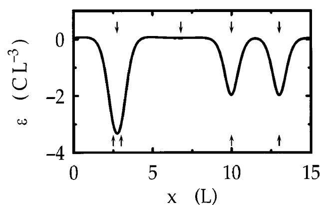

Fig. 6. Surfaces strain ε vs. lateral displacement x (in units of spacer thickness L), for four islands buried at depth L according to the calculation in [26]. Arrows at botttom indicate positions of buried islands. Arrows at top indicate minima in ε, i.e. favored for subsequent nucleation. Reprinted from [26] with the kind permission of the authors.

relative to pure Si, such that the lattice parameter is closer to that of the SiGe alloy. The energy cost of nucleating a coherently strained island at these strain minima is smaller than in regions between islands, where the Si spacer layer is closer to its bulk equilibrium value [26].

Fig. 6 shows the results of such a calculation: the strain field at the surface as a function of lateral position above a buried layer of islands. The two right-hand islands are far enough apart that they each give rise to a minimum in the strain field at the top, exposed surface. Islands that are very close together, such as the two left-most islands in Fig. 6, give rise to a single minimum, centered between the two islands, causing a single island to form above the island pair. The distance over which strain fields interact is determined primarily by the spacer-layer thickness [26]. Thus if this thickness is kept constant, island sizes must eventually reach a ‘stable’ size beyond which they will no longer merge with one another.

This model can be used to explain almost all of the phenomena shown in Fig. 5. The approach of two islands toward each other, island mergers, and the stabilization of island sizes after such mergers are all expected from interactions of strain fields of buried islands. Simulations, based on the calculated strain fields and deterministic rules for nucleation, give similar results to Figs. 4 and 5 [26].

Using TEM, Kienzle et al. [32] experimentally determined the degree of vertical correlation as a function of spacer layer thickness in the Ge/Si system. They show that spacer layer thicknesses between 12.5 and 25 nm result in the largest percentage of vertically correlated islands. In addition, they observed a ‘critical’ spacer layer thickness of 70 nm, beyond which islands have a probability of less than 1/2 of being vertically aligned with buried dots. Similar results were obtained for InAs/GaAs by Xie et al. [30]. For this system, the probability for islands to be vertically correlated with islands in other layers begins to decrease at a spacer layer thickness of approximately 50 nm and falls to 1/2 at about 90 nm.

Vertical correlation can manifest itself in more complex ways than that shown in Fig. 5. For example, anticorrelation, in which islands in adjacent layers are laterally shifted with respect to one another, has also been observed [37]. In PbSe/$Pb_{1-x}Eu_xTe$ multilayers [38], 3D islands in adjacent layers are positioned according to FCC stacking rules. These effects are qualitatively understood in terms of the model described above: preferred nucleation sites are determined by the strain field from buried islands. Due to the anisotropic elastic properties of real crystals, preferred nucleation sites are not necessarily located above buried islands [37].

3.2. Ordering in sparse arrays

The experiments and theory discussed above primarily involve multilayers with densely packed islands. For example, analysis of Fig. 5 and similar TEM data suggests that merging of islands is the dominant effect in the evolution of multilayer QD films. These mergers appear to cause the increased uniformity in island size: the distribution of 'daughter' islands (these are islands closer to the surface that lie above a pair of deeper islands) is noticeably narrower than that of the 'parent' islands. However, multilayers of sparse arrays of QDs (i.e. having a low number density), in which island mergers are rare, can also exhibit a narrowing size distribution with increasing layer number. In these systems, the island density is approximately constant [30,33], so that the narrowing island size distribution cannot be explained by island mergers. In addition, because buried islands in the model represented by Fig. 6 are considered spherical, no explanation of the evolution from rectangular to square islands shown in Fig. 4 can be expected.

In order to explain these aspects of multilayer QD ordering, Liu et al. [39] performed deterministic simulations, resembling those in [26], but based on strain fields from more realistic shapes for the buried islands. One of the principal analytical results of this calculation is the dependence of the extent, x_0, of the tensile region of the strain field at the spacer layer surface on the width, W, of the buried island. In particular, x_0 is always larger than W and is proportional to $W^{1/2}$.

In their simulations, Liu et al. propose that the size of an island that nucleates in a region of tensile strain is fully determined by the size of this strained region. In particular, they fix the ratio of new island size, B_i, to tensile region, x_0, at some value less than unity. This assumption, combined with the dependence of x_0 on W, leads to a critical island size toward which all islands will evolve [39].

The same mechanism also explains the approach toward square islands described above. In particular, when an anisotropic island is buried, it produces a tensile region that is also anisotropic. However, the aspect ratio of the tensile region, which determines that of the new island, is reduced relative to that of the original island [39]. Thus the island size approaches a more isotropic shape. Fig. 7 shows the evolution of a single island column, in a 3D simulation of multilayer film growth, for which the island's initial aspect ratio is 4:1. After about 12 layers, the aspect ratio has evolved to nearly 1:1.

3.3. Multilayer engineering

Knowledge of SK growth in single, strained heteroepitaxial layers and multilayer ordering provides additional means of control of the properties of ensembles of coherent, 3D islands. Mukhametzhanov et al. [31] demonstrated how to control independently the size and density of InAs/GaAs islands in a bilayer. The first layer is intentionally grown with a low density of islands, approximately 3.7×10^{10} cm^{-2}. Next a spacer layer is grown, followed by a second layer. The amount of deposited material in the second layer is larger than that of the first layer. In the absence of the buried layer, this larger coverage results in an island density of 9.0×10^{10} cm^{-2}. Due to the strain inhomogeneity arising from the buried layer, the island density is only 4.8×10^{10} cm^{-2}. Furthermore, the island size distribution in the second layer is slightly narrower than that of the buried layer.

A common observation among samples of multilayer Ge/Si QD arrays is that, even with a constant amount of Ge deposited in each layer, the islands become larger with increasing layer number. This increase in size is primarily caused by a concomitant decrease in island density, as is evident from Figs. 4 and 5. However, careful study [40,41] of multilayer structures reveals that the wetting-layer thickness decreases with increasing layer number, giving rise to an increase in average island size with increasing layer number even when the island density remains constant. For Ge/Si heterostructures with a 2.5 nm Si spacer layer, the measured wetting-layer thickness changes from 4 ml for the first Ge layer to about 1.66 ml in the second Ge layer [40]. In this experiment, sparse arrays of islands were used so that the island density was the same for all layers. In order to produce equal sized quantum dots among different layers, Thanh et al. compensated for this reduction in wetting-layer thickness by reducing the total Ge dose with increasing layer number [40].

4. Summary and outlook

In this chapter we have described the spontaneous formation, or self-assembly, of 3D islands in strained, heteroepitaxial, semiconductor thin films. Such islands are dislocation-free, have lateral dimensions on the order of 10 nm, and form in a wide variety of systems, including Ge/Si and InAs/GaAs, making them promising candidates for semiconductor QDs. Coherent, 3D islands form via the Stranski–Krastanov growth mode, in which the deposited material initially wets the substrate, but forms islands after a system-dependent critical thickness. Strain can alter both the kinetics and equilibrium properties that govern island evolution, producing dramatic affects on island nucleation and coarsening phenomena, and also on the size and size distributions of islands within a strained layer. Research on semiconductor QDs has begun to focus on ways to manipulate and engineer 3D islands and island distribu-

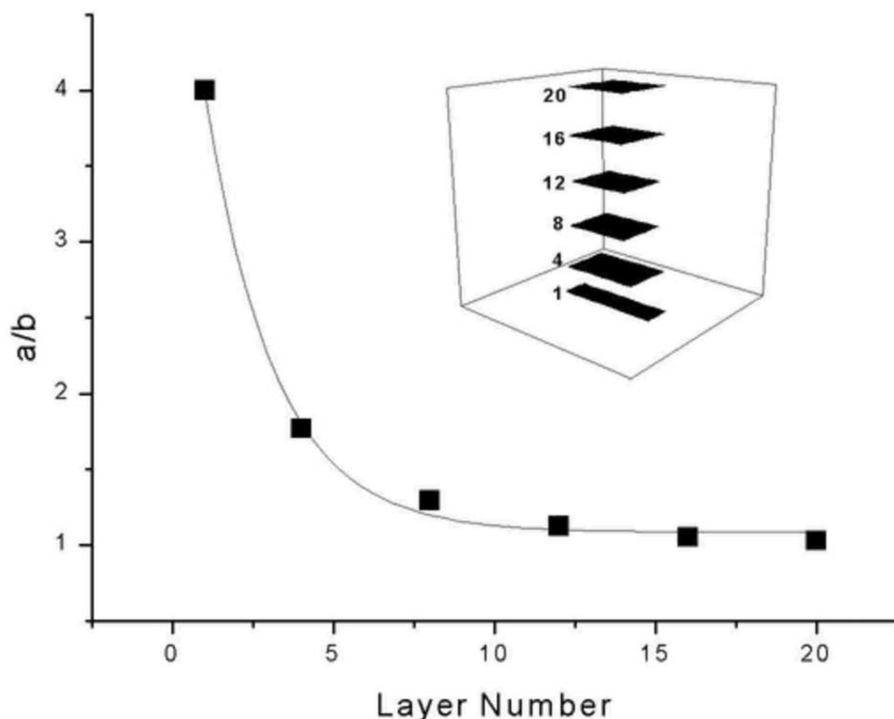

Fig. 7. Evolution of the aspect ratio a/b of base dimensions of 3D islands in a multilayer film of 20 bilayers simulated for a single island column. The solid line is a guide to the eye. The inset shows a schematic view of the island shape evolution.

tions for use in devices. Such methods include substrate patterning, vicinal and step-bunched substrates, dislocation arrays, multilayers, and combinations of these techniques. Fundamental aspects of Stranski–Krastanov growth play a large role in developing such methods. We expect these developments to lead to increasing use of semiconductor quantum dots in novel and established micro- and optoelectronics technologies.

Acknowledgements

We thank Don Savage for many helpful discussions. Preparation of this review was supported by DARPA, ONR, and NSF.

References

[1] J. Drucker, S. Chaparro, Appl. Phys. Lett. 71 (1997) 614.
[2] F.M. Ross, J. Tersoff, R.M. Tromp, Phys. Rev. Lett. 80 (1998) 984.
[3] D. Leonard, K. Pond, P.M. Petroff, Phys. Rev. B 50 (1994) 11687.
[4] N.P. Kobayashi, T.R. Ramachandran, P. Chen, A. Madhukar, Appl. Phys. Lett. 68 (1996) 3299.
[5] M. Pinczolits, G. Springholz, G. Bauer, Appl. Phys. Lett. 73 (1998) 250.
[6] V.A. Shchukin, D. Bimberg, Rev. Mod. Phys. 71 (1999) 1125.
[7] B. Lewis, J.C. Anderson, Nucleation and Growth of Thin Films, Academic Press, New York, 1978.
[8] J.S. Sullivan, E. Mateeva, H. Evans, D.E. Savage, M.G. Lagally, J. Vac. Sci. Technol. A 17 (1999) 2345.
[9] T.R. Ramachandran, A. Madhukar, I. Mukhametzhanov, R. Heitz, A. Kalburge, Q. Xie, P. Chen, J. Vac. Sci. Technol. B 16 (1998) 1330.
[10] J.S. Sullivan, Ph.D. thesis, University of Wisconsin, Madison, 1999.
[11] C. Hernandez, Y. Campidelli, D. Simon, D. Bensahel, I. Sagnes, G.B. Patriarche, S. Sauvage, J. Appl. Phys. 86 (1999) 1145.
[12] G. Abstreiter, P. Schittenhelm, C. Engel, E. Silveira, A. Zrenner, D. Meertens, Sem. Sci. Technol. 11 (1996) 1521.
[13] G. Jin, J.L. Liu, S.G. Thomas, Y.H. Luo, K.L. Wang, B.Y. Nguyen, Appl. Phys. Lett. 75 (1999) 2752.
[14] G. Jin, J. Wan, Y.H. Luo, J.L. Liu, K.L. Wang, J. Cryst. Growth 227–228 (2001) 1100.
[15] T.I. Kamins, R.S. Williams, D.P. Basile, Nanotechnology 10 (1999) 117.
[16] T.I. Kamins, D.A.A. Ohlberg, R.S. Williams, W. Zhang, S.Y. Chou, Appl. Phys. Lett. 74 (1999) 1773.
[17] T.L. Kamins, R.S. Williams, Appl. Phys. Lett. 71 (1997) 1201.
[18] K.H. Ploog, R. Nötzel, Thin Solid Films 367 (2000) 32.
[19] P. Rugheimer, E. Mateeva, D.E. Savage, M.G. Lagally (2001) in preparation.
[20] C. Teichert, J.C. Bean, M.G. Lagally, Appl. Phys. A 67 (1998) 675.
[21] C. Teichert, J. Barthel, H.P. Oepen, J. Kirschner, Appl. Phys. Lett. 74 (1999) 588.
[22] H. Omi, T. Ogino, Phys. Rev. B 59 (1999) 7521.
[23] H. Omi, T. Ogino, Thin Solid Films 369 (2000) 88.
[24] C. Teichert, C. Hofer, K. Lyutovich, M. Bauer, E. Kasper, Thin Solid Films 380 (2000) 25.
[25] A. Konkar, R. Heitz, T.R. Ramachandran, P. Chen, A. Madhukar, J. Vac. Sci. Technol. B 16 (1998) 1334.
[26] J. Tersoff, C. Teichert, M.G. Lagally, Phys. Rev. Lett. 76 (1996) 1675.
[27] C. Teichert, M.G. Lagally, L.J. Peticolas, J.C. Bean, J. Tersoff, Phys. Rev. B 53 (1996) 16334.

[28] E. Mateeva, P. Suttler, J.C. Bean, M.G. Lagally, Appl. Phys. Lett. 71 (1997) 3233.
[29] A.A. Darhuber, P. Schittenhelm, V. Holy, J. Stangl, G. Bauer, G. Abstreiter, Phys. Rev. B 55 (1997) 15652.
[30] X. Qianghua, A. Madhukar, P. Chen, N.P. Kobayashi, Phys. Rev. Lett. 75 (1995) 2542.
[31] I. Mukhametzhanov, R. Heitz, J. Zeng, P. Chen, A. Madhukar, Appl. Phys. Lett. 73 (1841) 1998.
[32] O. Kienzle, F. Ernst, M. Rühle, O.G. Schmidt, K. Eberl, Appl. Phys. Lett. 74 (1999) 269.
[33] M.K. Zundel, A.P. Specht, K. Eberl, N.Y. Jin-Phillip, F. Phillipp, Appl. Phys. Lett. 71 (1997) 2972.
[34] B. Damilano, N. Grandjean, F. Semond, J. Massies, M. Leroux, Appl. Phys. Lett. 75 (1999) 962.
[35] T.S. Kuan, S.S. Iyer, Appl. Phys. Lett. 59 (1991) 2242.
[36] J.Y. Yao, T.G. Andersson, G.L. Dunlop, J. Appl. Phys. 69 (1991) 2224.
[37] V.A. Shchukin, D. Bimberg, V.G. Malyshkin, N.N. Ledentsov, Phys. Rev. B 57 (1998) 12262.
[38] G. Springholz, V. Holy, M. Pinczolits, G. Bauer, Science 282 (1998) 734.
[39] F. Liu, S.E. Davenport, H.M. Evans, M.G. Lagally, Phys. Rev. Lett. 82 (1999) 2528.
[40] V.L. Thanh, V. Yam, P. Boucaud, Y. Zheng, D. Bouchier, Thin Solid Films 369 (2000) 43.
[41] O.G. Schmidt, O. Kienzle, Y. Hao, K. Eberl, F. Ernst, Appl. Phys. Lett. 74 (1999) 1272.